Supporting Information

for

Photophysical Characterization of a Helical Peptide Based Chromophore–Water Oxidation Catalyst Assembly on a Semiconductor Surface Using Ultrafast Spectroscopy

Stephanie E. Bettis, Derek M. Ryan, Melissa K. Gish, Leila Alibabaei, Thomas J. Meyer, Marcey L. Waters, John M. Papanikolas*

Department of Chemistry, CB 3290, University of North Carolina, Chapel Hill, NC 27599

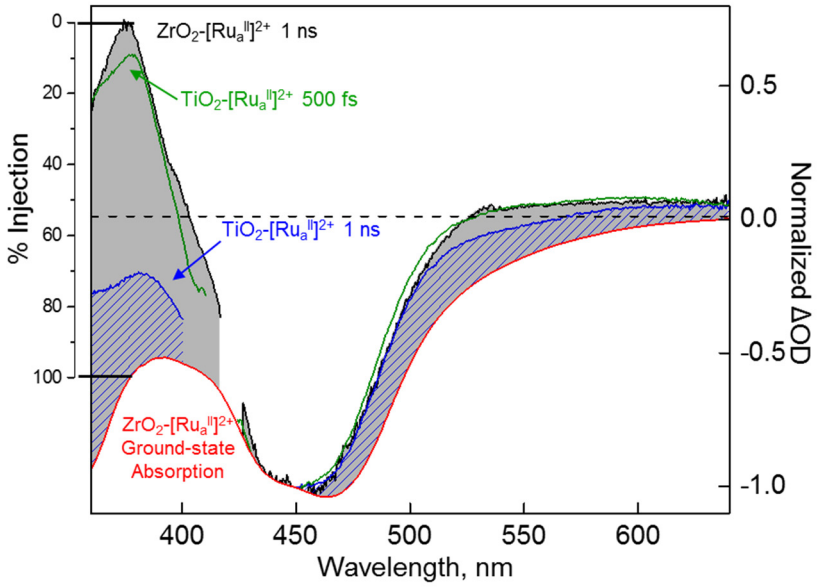

Figure S1. The electron injection efficiency for TiO_2-$[Ru_a^{II}]^{2+}$ is calculated from the ratio of the difference between the transient absorption intensity at 380 nm of $[Ru_a^{II}]^{2+}$ on TiO_2 (blue) and ZrO_2 (black) at 1 ns and the difference between intensity of ZrO_2 at 1 ns (black) and the inverse of the ground state absorption on ZrO_2 (red) at 380 nm. The electron injection efficiency for TiO_2-Ru_a^{II} is 72%. The 9% ultrafast injection is seen in the ratio between ZrO_2-$[Ru_a^{II}]^{2+}$ (black) and TiO_2-$[Ru_a^{II}]^{2+}$ at 500 fs (green). These efficiencies are used to determine the initial concentrations of $[\text{-}Ru_a^{II}\text{*-}]^{2+}$ and $[\text{-}Ru_a^{III}\text{-}]^{3+}$ in the global analysis.

Table S1. Summary of fit for electron injection kinetics at 380 nm of $[Ru_a^{II}]^{2+}$, $[Ru_a^{II}\text{-}Ru_b^{II}\text{-}OH_2]^{4+}$, and $[Ru^{II}(pbpy)_2(bpy)]^{2+}$ on TiO_2 and ZrO_2.

	A_1	τ_1	A_2	τ_2	Offset
TiO_2-$[Ru_a^{II}]^{2+}$	0.59 ± 0.31	19.3 ± 1.5	0.69 ± 0.03	201.7 ± 18.5	-0.34 ± 0.14
ZrO_2-$[Ru_a^{II}]^{2+}$	0.03 ± 0.02	9.7 ± 17.6	--	--	0.87 ± 0.12
TiO_2-$[Ru^{II}(pbpy)_2(bpy)]^{2+}$	0.71 ± 0.20	14.3 ± 4.3	0.46 ± 0.20	77.5 ± 36.1	-0.33 ± .02
TiO_2-$[Ru_a^{II}\text{-}Ru_b^{II}\text{-}OH_2]^{4+}$	0.57 ± 0.02	6.85 ± 0.55	0.53 ± 0.02	77.10 ± 6.44	-0.11 ± 0.07
ZrO_2-$[Ru_a^{II}\text{-}Ru_b^{II}\text{-}OH_2]^{4+}$	0.33 ± 0.02	101.3 ± 23.7	--	--	0.55 ± 0.02

Table S2. Summary of the fits of time-resolved emission for ZrO_2-$[Ru_a^{II}]^{2+}$ and ZrO_2-$[Ru_a^{II}$-Ru_b^{II}-$OH_2]^{4+}$.

	A_1	k_1, $x10^6$ s^{-1} (τ_1,ns)	A_2	k_1, $x10^6$ s^{-1} (τ_2, ns)	Average k_1, $x10^6$ s^{-1} (τ, ns)
ZrO_2-$[Ru_a^{II}]^{2+}$	0.4 ± 0.01	14.2 ± 0.2 (70.4 ± 1.0)	0.6 ± 0.01	2.57 ± 0.01 (389 ± 1.4)	3.82 ± 0.02 (261.5 ± 1.2)
ZrO_2-$[Ru_a^{II}$-Ru_b^{II}-$OH_2]^{4+}$	0.87 ± 0.01	73.6 ± 1.1 (13.6 ± 0.2)	0.13 ± 0.01	14.3 ± 0.4 (70.0 ± 2.1)	47.8 ± 0.9 (20.9 ± 0.4)

Table S3. Summary of the fit to the change in wavelength of the bleach (at 50% point) for TiO_2-$[Ru_a^{II}]^{2+}$ and TiO_2-$[Ru_a^{II}$-Ru_b^{II}-$OH_2]^{4+}$.

	A_1	τ_1 (ps)	A_2	τ_2 (ps)
TiO_2-$[Ru_a^{II}]^{2+}$	1 ± 0.05	80.84 ± 12.34	--	--
TiO_2-Ru_a^{II}-Ru_b^{II}	0.3 ± 0.03	25.51 ± 3.89	0.7 ± 0.03	342.91 ± 48.52

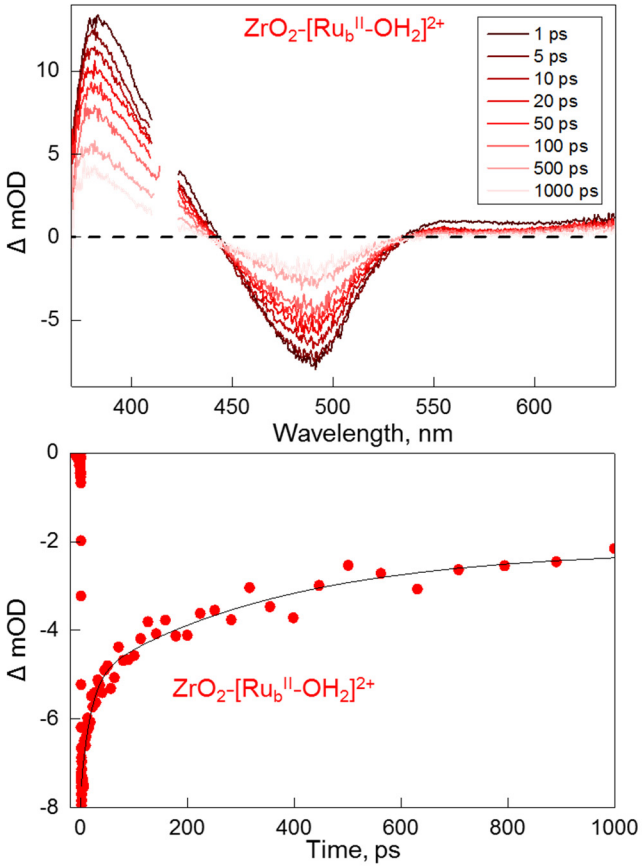

Figure S2. a) Transient absorption spectra of ZrO_2-[Ru(4,4'-$(CH_2PO_3H_2)_2$bpy)(mebimpy)$(H_2O)]^{2+}$ from 1 ps (dark line) to 1 ns (light line) after laser excitation. b) Transient absorption kinetics of ZrO_2-[Ru(4,4'-$(CH_2PO_3H_2)_2$bpy)(mebimpy)$(H_2O)]^{2+}$ at 490 nm. The biexponential fit (black line) has an offset of -2.2 and two time components 5.45 x 10^{10} s^{-1}, 18.3 ps (-2.4) and 2.75 x 10^9 s^{-1}, 363.6 ps (-3.0). The fast component is due to vibrational relaxation on ZrO_2 surface and the long component is the catalyst excited-state decay. The sample was on 3 μm thick nanocrystalline ZrO_2 in aqueous 0.1 M $HClO_4$ at 25 °C. The excitation wavelength was 420 nm.

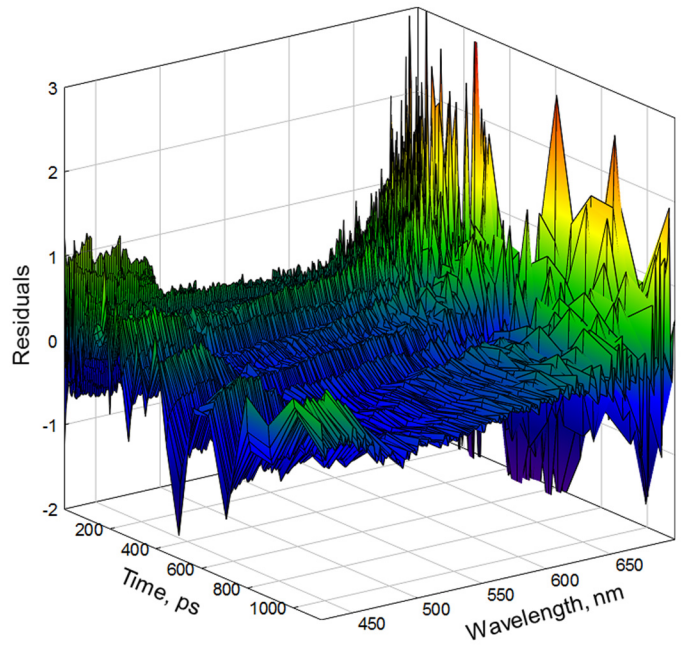

Figure S3. Residuals from the global analysis of TiO_2-$[Ru_a^{II}]^{2+}$.

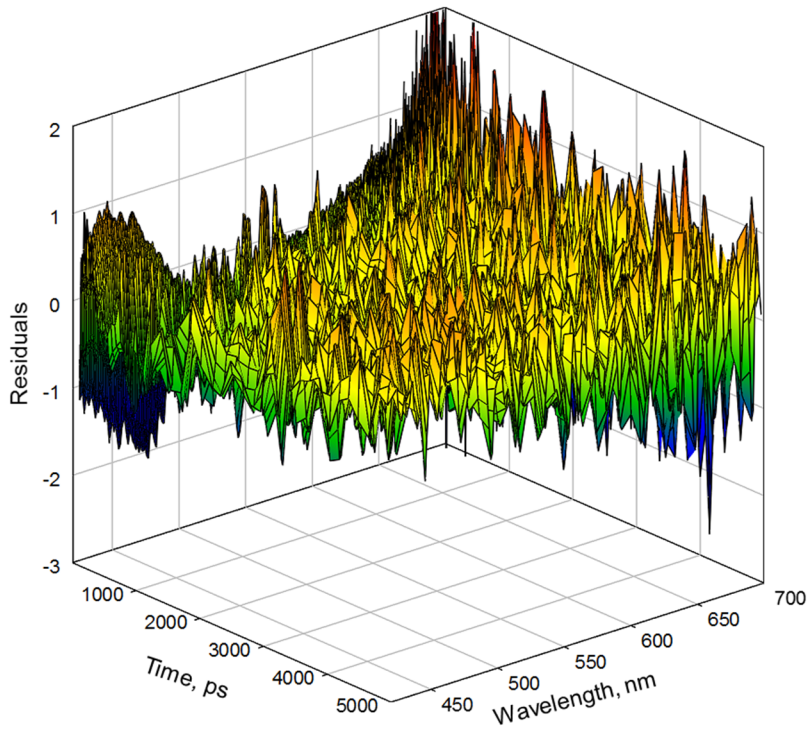

Figure S4. Residuals from the global analysis of TiO_2-$[Ru_a^{II}$-Ru_b^{II}-$OH_2]^{4+}$.